A FINITE ELEMENT METHOD FOR POISSON'S EQUATION

by
Stephen V. Harren
http://www.harren.us

0. Contents

1. Governing Equations

The simplest second-order elliptic partial differential equation is Poisson's equation, *viz.,*

$$T\nabla^2 u + p = 0\,, \tag{1.1}$$

where u is the transverse displacement of a (*e.g.,* soap) film, p is the transverse pressure, and T is the surface tension of the film (force per unit length). In Cartesian coordinates, the Laplacian is

$$\nabla^2 u = u_{,ii} = u_{,xx} + u_{,yy}\ , \tag{1.2}$$

where the comma denotes partial differentiation with respect to the coordinates.

In polar coordinates we have

$$\nabla^2 u = u_{,rr} + \frac{1}{r}u_{,r} + \frac{1}{r^2}u_{,\theta\theta}\ . \tag{1.3}$$

Also in polar coordinates, the components of the gradient are

$$(\boldsymbol{\nabla} u)_r = u_{,r}\ , \qquad (\boldsymbol{\nabla} u)_\theta = \frac{1}{r}u_{,\theta}\ . \tag{1.4}$$

Attention is now given to the Principle of Virtual Work. Thus, let u^* be a once-differentiable scalar field (the so-called virtual displacement). By the product rule of differentiation

$$\left(u^* u_{,i}\right)_{,i} = u^*_{,i} u_{,i} + u^* u_{,ii}\ . \tag{1.5}$$

Now, substituting of eqns. (1.1) and (1.2) into eqn. (1.5), one obtains

$$T u^*_{,i} u_{,i} = T\left(u^* u_{,i}\right)_{,i} + u^* p\,. \tag{1.6}$$

Next, integrate eqn. (1.6) over the domain A and use the Divergence Theorem to see

$$T\int_A u^*_{,i} u_{,i}\,\mathrm{d}A = T\oint_t u^* u_{,n}\,\mathrm{d}t + \int_A u^* p\,\mathrm{d}A\ , \tag{1.7}$$

which is the Principle of Virtual Work. In eqn. (1.7), t is the coordinate around the boundary of A, and $u_{,n} = n_i u_{,i}$ is the normal derivative of u ($\mathbf{n}$ is the outward-pointing unit normal vector on the boundary). From eqn. (1.7) we see that admissible boundary conditions for Poisson's equation are prescribe either u or $u_{,n}$ at each point on the boundary.

2. Example in Rectangular Coordinates

Consider the $L \times H$ rectangular domain, pictured in Fig. 1, subjected to the "bubble" pressure distribution

$$p = p_0 \cos\left(\frac{\pi x}{L}\right)\cos\left(\frac{\pi y}{H}\right), \tag{2.1}$$

where p_0 is the pressure at the origin. The boundary conditions are

$$u = 0 \tag{2.2}$$

on all four faces. Here, the governing equation is, *cf.,* eqns. (1.1) and (1.2),

$$u_{,xx} + u_{,yy} = -\frac{1}{T}p_0 \cos\left(\frac{\pi x}{L}\right)\cos\left(\frac{\pi y}{H}\right). \tag{2.3}$$

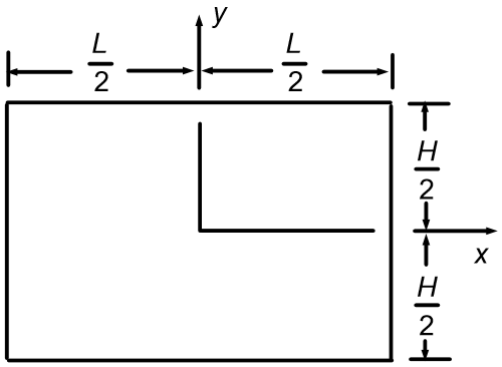

Figure 1. Rectangular domain as described in the text.

Equation (2.3) is solved with a displacement of the form

$$u = k\cos\left(\frac{\pi x}{L}\right)\cos\left(\frac{\pi y}{H}\right). \tag{2.4}$$

Note that eqn. (2.4) satisfies the boundary conditions (2.2). In any case, substituting eqn. (2.4) into eqn. (2.3) yields the value of k, *viz.,*

$$k = \frac{p_0}{\pi^2 T}\left(\frac{L^2H^2}{L^2+H^2}\right). \tag{2.5}$$

Also, the gradients are

$$u_{,x} = -k\frac{\pi}{L}\sin\left(\frac{\pi x}{L}\right)\cos\left(\frac{\pi y}{H}\right), \qquad u_{,y} = -k\frac{\pi}{H}\cos\left(\frac{\pi x}{L}\right)\sin\left(\frac{\pi y}{H}\right). \tag{2.6}$$

3. Example in Polar Coordinates

Consider the quarter-annular domain shown in Fig. 2 subjected to the pressure load

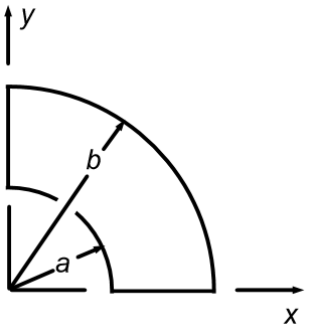

Figure 2. Quarter-annular domain as described in the text.

$$p = \frac{2F}{b^2-a^2}\cos\theta, \tag{3.1}$$

where F is the net force acting on the domain, *i.e.,*

$$F = \int_A p\,\mathrm{d}A. \tag{3.2}$$

In this case the governing equation is

$$u_{,rr} + \frac{1}{r}u_{,r} + \frac{1}{r^2}u_{,\theta\theta} = -\frac{2F}{T(b^2-a^2)}\cos\theta, \tag{3.3}$$

cf., eqns. (1.1) and (1.3). The boundary conditions for the problem are

$$u_{,n} = 0 \text{ on } \theta = 0, \quad \text{and} \quad u = 0 \text{ on the other three boundaries.} \tag{3.4}$$

Assuming a displacement of the form

$$u = f(r)\cos\theta \tag{3.5}$$

eqn. (3.3) becomes

$$f'' + \frac{1}{r}f' - \frac{1}{r^2}f = -\frac{2F}{T(b^2-a^2)}, \tag{3.6}$$

whose general solution is

$$f = k_1 r + \frac{k_2}{r} - \frac{2F}{3T(b^2-a^2)}r^2, \qquad f' = k_1 - \frac{k_2}{r^2} - \frac{4F}{3T(b^2-a^2)}r. \tag{3.7}$$

Also, from eqns. (1.4), the components of the gradient vector are

$$(\boldsymbol{\nabla} u)_r = f'(r)\cos\theta \ , \qquad (\boldsymbol{\nabla} u)_\theta = -\frac{1}{r} f(r)\sin\theta \ . \tag{3.8}$$

Finally, one notes, from eqns. (3.5) and the second of eqns. (3.8), that the boundary conditions are satisfied identically on the faces $\theta = 0$ and $\theta = \pi/2$. Then, satisfying the boundary conditions on $r = a$ and $r = b$ gives the values of the constants

$$k_1 = \frac{2F(b^3 - a^3)}{3T(b^2 - a^2)^2} \ , \qquad k_2 = -\frac{2Fa^2b^2(b-a)}{3T(b^2 - a^2)^2} \ , \tag{3.9}$$

which solves the problem at hand.

4. The 9–Noded Isoparametric Finite Element

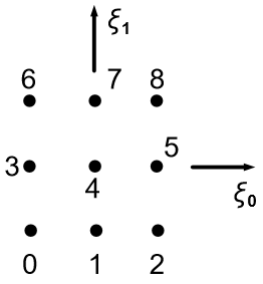

Figure 3. The 9–noded isoparametric finite element in **ξ**–space as explained in the text.

At left in Fig.3 is pictured the finite element in normalized **ξ**–space spanning $(-1,1)\times(-1,1)$. The geometry of the element in physical **x**–space is interpolated with the aid of the quadratic functions

$$\begin{aligned} a^0 &= \frac{1}{2}(-\xi + \xi^2) \\ a^1 &= 1 - \xi^2 \\ a^2 &= \frac{1}{2}(\xi + \xi^2) \ , \end{aligned} \tag{4.1}$$

the tensor product of which functions yield the desired interpolation functions S^I, *viz.,*

$$\begin{array}{lll} S^0 = a^0(\xi_0)a^0(\xi_1) & S^1 = a^1(\xi_0)a^0(\xi_1) & S^2 = a^2(\xi_0)a^0(\xi_1) \\ S^3 = a^0(\xi_0)a^1(\xi_1) & S^4 = a^1(\xi_0)a^1(\xi_1) & S^5 = a^2(\xi_0)a^1(\xi_1) \ , \\ S^6 = a^0(\xi_0)a^2(\xi_1) & S^7 = a^1(\xi_0)a^2(\xi_1) & S^8 = a^2(\xi_0)a^2(\xi_1) \end{array} \tag{4.2}$$

which are the usual "shape" functions of the 9–noded isoparametric finite element. Notwithstanding, the physical coordinates and pressure are interpolated via

$$x_i = S^I x_i^I \ , \qquad p = S^I p^I \ , \tag{4.3}$$

where x_i^I are the physical coordinates of the nodes, and p^I are the pressures at those nodes. Now, differentiation of the first of eqns. (4.3) gives

$$\frac{\partial x_i}{\partial \xi_\alpha} = S^I_{,\alpha} x_i^I \equiv A_{i\alpha} \ , \qquad \mathrm{d}x_i = A_{i\alpha}\mathrm{d}\xi_\alpha \ , \qquad \mathrm{d}A_{\mathbf{x}} = (\det \mathbf{A})\mathrm{d}A_{\boldsymbol{\xi}} \ , \tag{4.4}$$

where $\mathrm{d}A_{\mathbf{x}}$ is the differential of area in **x**–space, and $\mathrm{d}A_{\boldsymbol{\xi}}$ is the differential of area in **ξ**–space. Thus,

$$\int_{A_{\mathbf{x}}} (\ )\mathrm{d}A_{\mathbf{x}} = \int_{A_{\boldsymbol{\xi}}} (\ )\,(\det \mathbf{A})\mathrm{d}A_{\boldsymbol{\xi}} \ . \tag{4.5}$$

In the numerical calculations, area integrations like (4.5) are carried out numerically via the 3–point Gauss-Legendre quadrature rule, which integrates a fifth order polynomial exactly. Finally, from the second of eqns. (4.4)

$$\mathrm{d}\xi_\alpha = A^{-1}_{\alpha i}\mathrm{d}x_i \ , \qquad S^I_{,i} = S^I_{,\alpha} A^{-1}_{\alpha i} \ , \tag{4.6}$$

which gives the gradients of the shape functions in **x**–space.

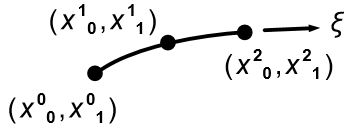

Figure 4. A face of the element.

Figure 4 shows one of the faces of the element (with renumbering of the nodes, as needed). Again, the normalized coordinate $\xi \in (-1,1)$. Here

$$x_i = a^I x_i^I \qquad I = 0,1,2, \tag{4.7}$$

where a^I are as per eqns. (4.1). Now, defining B_i via

$$x_{i,\xi} = a^I_{,\xi} x_i^I \equiv B_i \quad \Rightarrow \quad \mathrm{d}x_i = B_i \mathrm{d}\xi \ . \tag{4.8}$$

Thus,

$$(\mathrm{d}t)^2 = \mathrm{d}x_i \mathrm{d}x_i \quad \Rightarrow \quad \mathrm{d}t = B\mathrm{d}\xi \ , \qquad B = \sqrt{B_i B_i} \ . \tag{4.9}$$

From eqns. (4.9) then, integrations over the boundary may be written as

$$\oint_t (\ )\,\mathrm{d}t = \int_{-1}^{1} (\ ) B \,\mathrm{d}\xi \ , \tag{4.10}$$

which line integrations, numerically, once again, are calculated with the 3–point Gauss-Legendre quadrature rule.

Attention is now turned to the Principle of Virtual Work (1.7). So, interpolate the virtual displacement within the element via

$$u^* = S^I u^{*I} \ , \qquad u^*_{,i} = S^I_{,i} u^{*I} \ , \tag{4.11}$$

where u^{*I} are the nodal values of the virtual displacement. Note that the first of eqns. (4.3) and (4.11) possess the same form. Hence the term "isoparametric". In any case, substitution of eqns. (4.11) into eqn. (1.7) gives

$$u^{*I} T \int_A S^I_{,i} u_{,i} \,\mathrm{d}A = u^{*I} T \oint_t S^I u_{,n} \,\mathrm{d}t + u^{*I} \int_A S^I p \,\mathrm{d}A \ , \tag{4.12}$$

or since u^{*I} is arbitrary,

$$T \int_A S^I_{,i} u_{,i} \,\mathrm{d}A = T \oint_t S^I u_{,n} \,\mathrm{d}t + \int_A S^I p \,\mathrm{d}A \ . \tag{4.13}$$

Next, interpolate u within the element with

$$u = S^J u^J \ , \qquad u_{,i} = S^J_{,i} u^J \ , \tag{4.14}$$

where u^J are the nodal values of the displacement u. Finally, putting eqns. (4.14) into eqn. (4.13) gives the stiffness relation for the element

$$K^{IJ} u^J = f_n^I + f_p^I \ , \tag{4.15}$$

where

$$K^{IJ} = T \int_A S^I_{,i} S^J_{,i} \,\mathrm{d}A \ , \qquad f_n^I = T \oint_t S^I u_{,n} \,\mathrm{d}t \ , \qquad f_p^I = \int_A S^I p \,\mathrm{d}A \ . \tag{4.16}$$

5. Numerical Example in Rectangular Coordinates

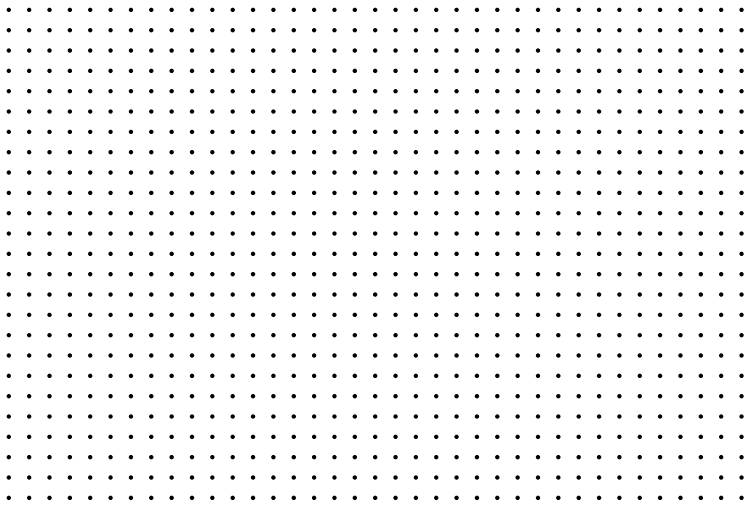

Figure 5. Computational grid used in the analysis as described in the text.

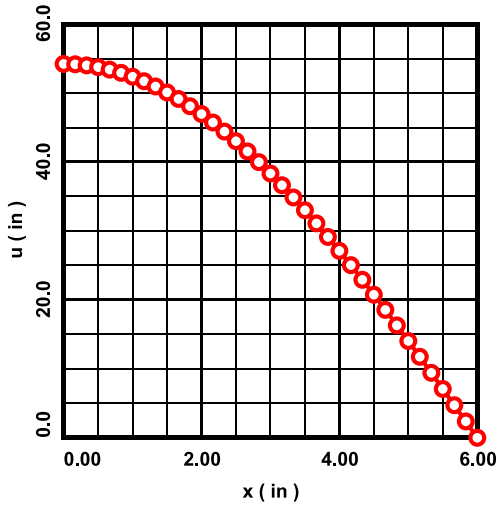

Figure 6. The displacement u at $y = 0$.

Here the problem presented above in **§2** is solved numerically. The computational grid used in the analysis is shown above in Fig. 5. It consists of a 37×25 array of nodes, and an 18×12 array of elements. Due to symmetry, only the upper right quadrant of the domain in Fig. 1 is analyzed. The corresponding boundary conditions at $x = 0$ and $y = 0$ are

$$u_{,n} = 0\,, \tag{5.1}$$

and the boundary conditions at $x = L/2$ and $y = H/2$ are

$$u = 0\,. \tag{5.2}$$

The constants used in the analysis are

$$T = 4.14 \times 10^{-4}\ \text{lb/in}\,, \quad L = 12\ \text{in}\,, \quad H = 8\ \text{in}\,, \quad p_0 = 5 \times 10^{-3}\ \text{psi}\,. \tag{5.3}$$

The value for T in eqns. (5.3) is for water, and as it turns out, the value used for p_0 is unrealistically large (very large displacements result).

Notwithstanding, in all the graphs herein: the solid curves represent the exact solution; and the plotted points, the numerically calculated results. The displacement u is calculated at the nodes of the grid, as are the displacement gradients $u_{,i}$ (by using the gradients of the element shape functions, and by using nodal averaging).

Figure 6 above shows the results for the displacement u at the bottom of the analyzed domain $y = 0$. The results for the displacement gradient $u_{,x}$, also at $y = 0$, are shown below in Fig. 7. Both the numerically calculated displacement and its gradient are highly accurate.

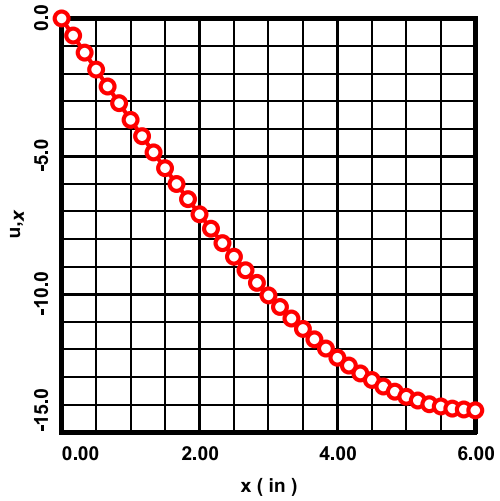

Figure 7. The displacement gradient $u_{,x}$ at $y = 0$.

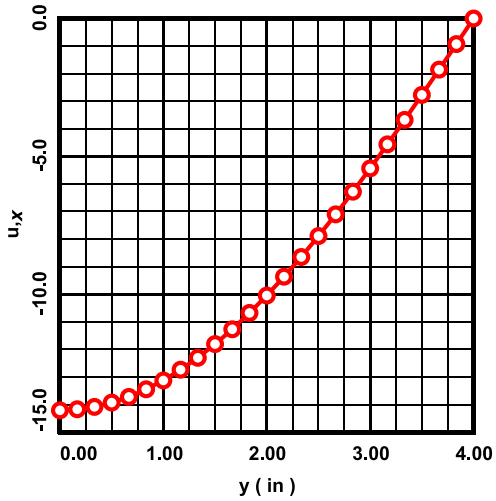

Figure 8. The displacement gradient $u_{,x}$ at $x = 6$ in.

The results for the displacement gradient $u_{,x}$ at the right boundary of the domain $x = 6$ in is shown above in Fig. 8. Once again, the numerically calculated results are highly accurate.

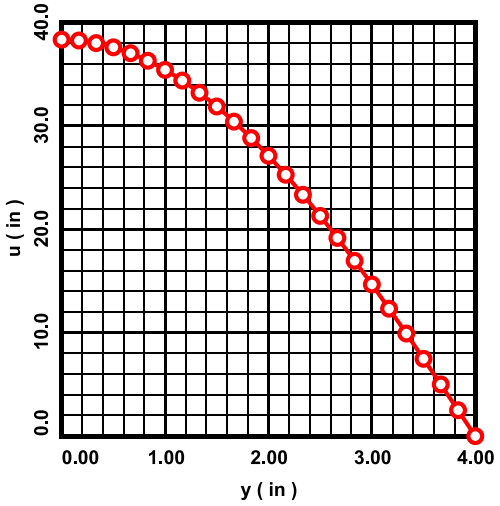

Figure 9. The displacement u at $x = 3$ in.

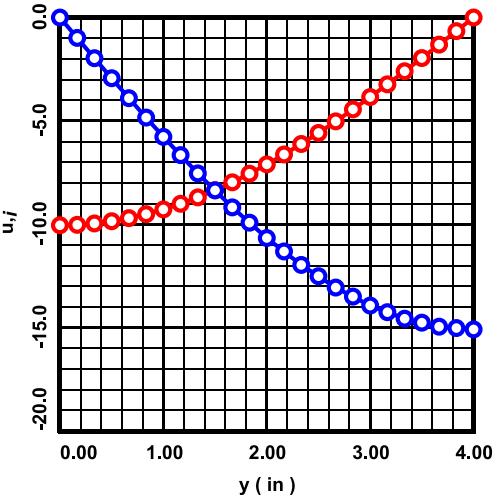

Figure 10. The displacement gradients $u_{,x}$ (red) and $u_{,y}$ (blue) at $x = 3$ in.

Finally, in Figs. 9 and 10 above are shown the calculated results along a vertical line of nodes in the grid located at $x = 3$ in. As has been the case, the numerically calculated values of the displacement u (Fig. 9) and the displacement gradients $u_{,i}$ (Fig. 10) basically coincide with the exact solution.

6. Numerical Example in Polar Coordinates

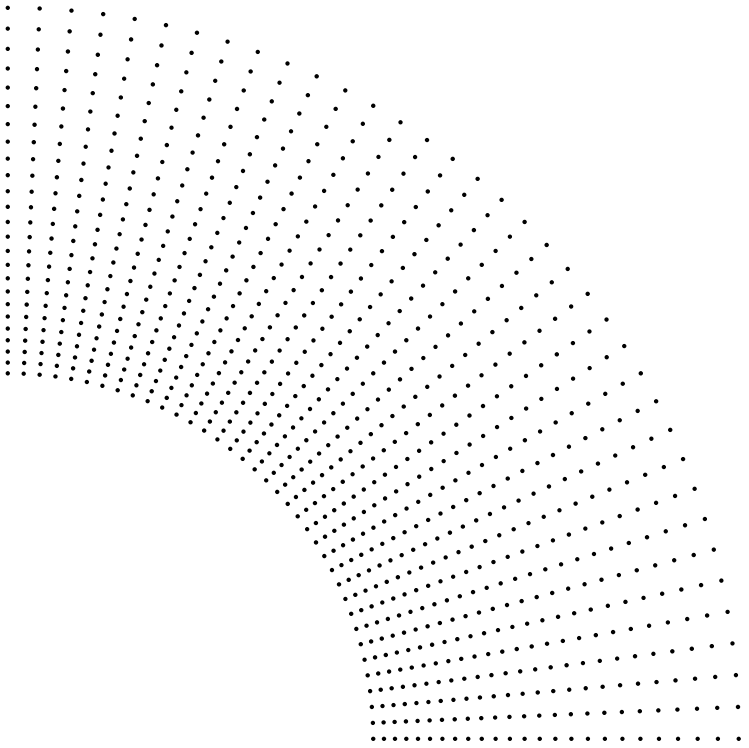

Figure 11. Computational grid used in the analysis as explained in the text.

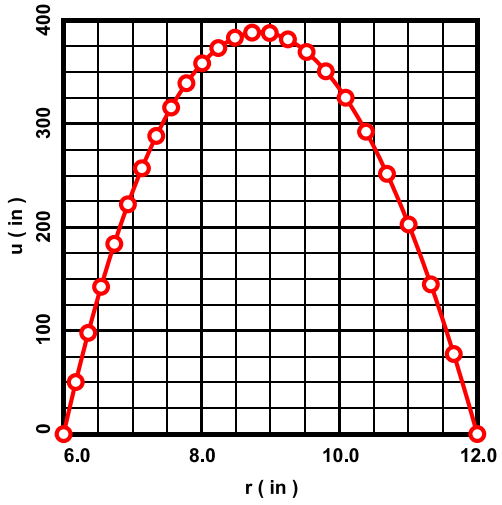

Figure 12. The displacement u at $\theta = 0$.

The problem solved analytically above in **§3** is analyzed here numerically. The computational grid used in the analysis is shown above in Fig. 11. It consists of a 25 (radial) × 37 (tangential) array of nodes, and a 12 (radial) × 18 (tangential) array of elements. The constants used in the analysis are

$$T = 4.14 \times 10^{-4} \text{ psi} , \quad F = 2.0 \text{ lb} ,$$
$$a = 6 \text{ in} , \quad b = 12 \text{ in} . \qquad (6.1)$$

The value of T in eqns. (6.1) is for water, and the value of F is unrealistically large (as was the case in **§5**, *i.e.,* unrealistically large displacements result).

In all the graphs herein: the solid curves represent the exact solution; and the plotted points, the numerically calculated results. The displacement u is calculated at the nodes of the grid, as are the displacement gradients $u_{,i}$ (by using the gradients of the element shape functions, and by using nodal averaging).

Figure 12 above shows the results for the displacement u at the bottom of the domain $\theta = 0$. Figure 13 below shows the displacement gradient $u_{,x}$ at the same location. As is evident, the numerically

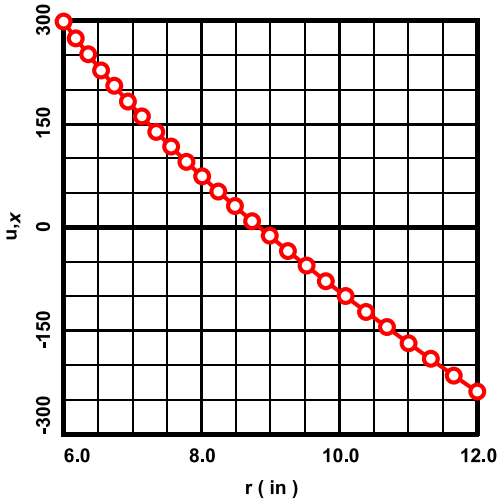

Figure 13. The displacement gradient $u_{,x}$ at $\theta = 0$.

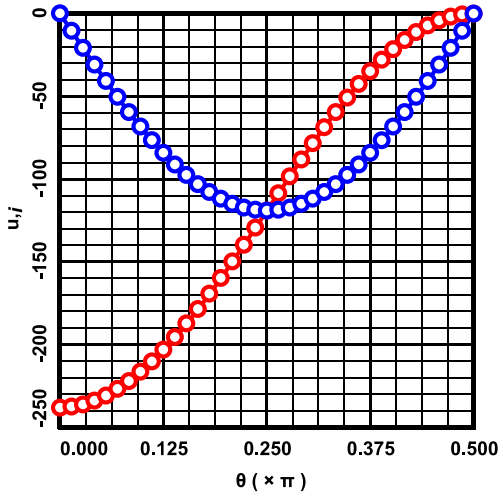

Figure 14. The displacement gradients $u_{,x}$ (red) and $u_{,y}$ (blue) at $r = 12$ in.

calculated results are highly accurate.

Figure 14 above shows the results for the displacement gradients $u_{,i}$ at the outer radius of the domain $r = 12$ in. Once again, the numerically calculated values are highly accurate.

Figure 15 below shows the results for the displacement gradient $u_{,x}$ at the left boundary of the domain $\theta = \pi/2$. As before, the numerically calculated results basically coincide with the exact solution.

The results for the displacement gradients $u_{,i}$ at the inner radius of the domain $r = 6$ in are shown below in Fig. 16. As previously, the numerically calculated results basically coincide with the exact solution.

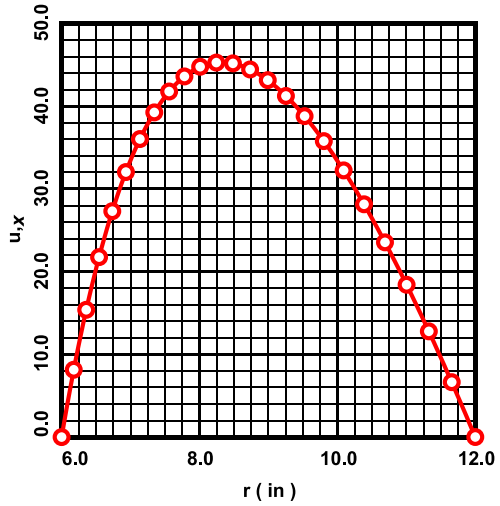

Figure 15. The displacement gradient $u_{,x}$ at $\theta = \pi/2$.

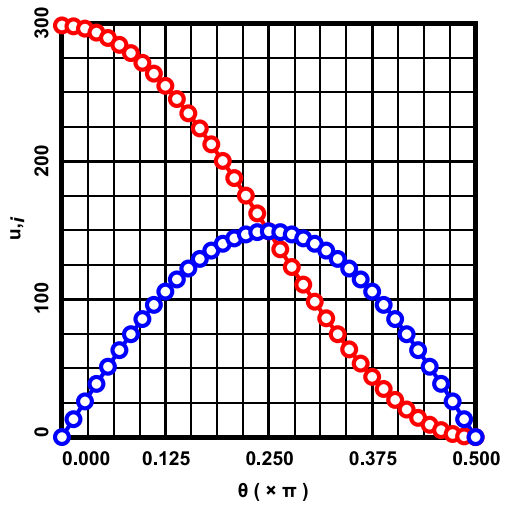

Figure 16. The displacement gradients $u_{,x}$ (red) and $u_{,y}$ (blue) at $r = 6$ in.

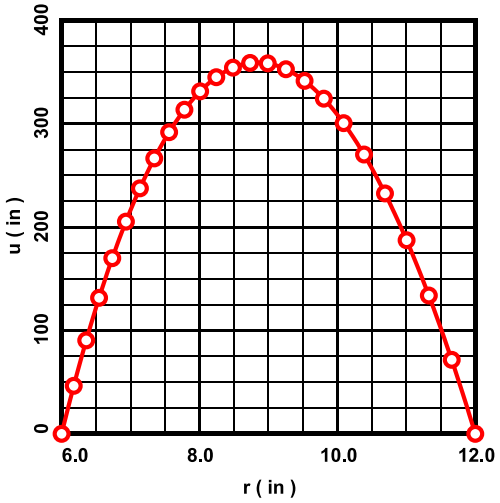

Figure 17. The displacement u at $\theta = \pi/8$.

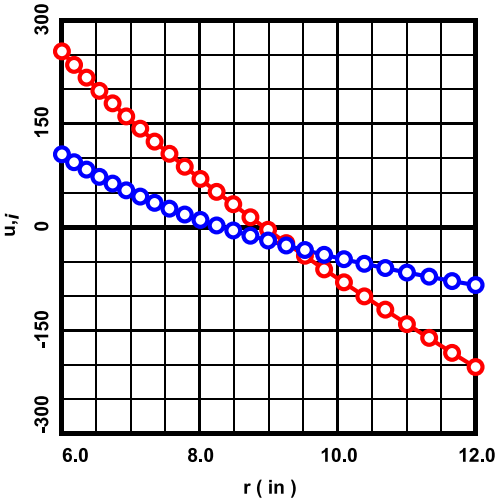

Figure 18. The displacement gradients $u_{,x}$ (red) and $u_{,y}$ (blue) at $\theta = \pi/8$.

The calculated results along a radial line of nodes through the grid located at $\theta = \pi/8$ are shown in Figs. 17 and 18 above. Yet again, the numerically calculated values of u (Fig.17) and $u_{,i}$ (Fig. 18) are highly accurate.

Finally, the numerical results for the displacement u and displacement gradients $u_{,i}$ along the ring of nodes in the grid located at $r = 9.253$ in are shown below in Figs. 19 and 20. As has been the case all along, the numerical results basically coincide with the exact solution.

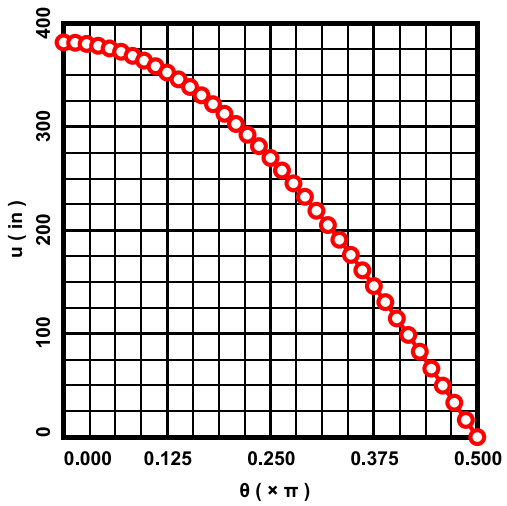

Figure 19. The displacement u at $r = 9.253$ in.

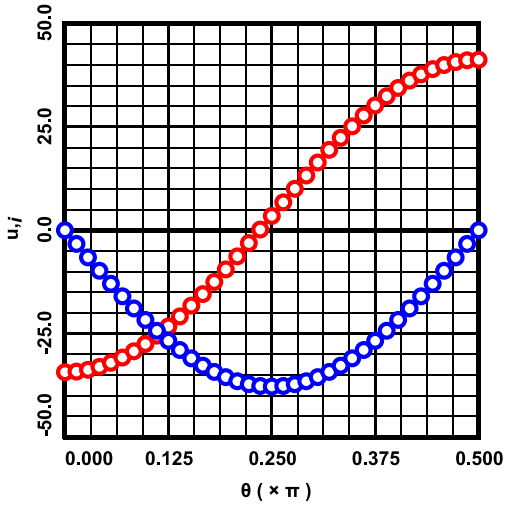

Figure 20. The displacement gradients $u_{,x}$ (red) and $u_{,y}$ (blue) at $r = 9.253$ in.

7. Closing Remarks

The above numerical results all are highly accurate. One reason for this is that Poisson's equation is very easy to solve. Another reason is that the 9–noded isoparametric finite element of **§4** is both very reliable and accurate. It is worth mentioning that if the grids shown above in Figs. 5 and 11 are meshed with 4–noded bi-linear isoparametric finite elements, then numerical results of comparable accuracy to those above are obtained.